Journal of Hydroscience and Hydraulic Engineering
Vol. 22, No.2 November, 2004, 93-104

FINITE-VOLUME MODEL FOR FLOOD FLOWS OVER SUBMERGED AND NON-SUBMERGED TOPOGRAPHY

By

Mirei Shige-eda and Juichiro Akiyama

Department of Civil Engineering, Kyushu Institute of Technology
Sensuicho 1-1, Tobata, Kitakyushu 804-8550, JAPAN

SYNOPSIS

A two-dimensional numerical model for flood flows in a flood plain with complicated topography is developed. The model is based on the Spatial Averaged Finite volume method on Unstructured grid using FDS technique for 2D Flood flows (SA-FUF-2DF model). An upwind treatment of bed slope terms and a procedure for the movement of a wet/dry boundary are incorporated into the SA-FUF-2DF model to treat flood flows on complicated topography. The model is first applied to an experiment of the solitary wave which passes around a conical island, and then is verified against the experimental data of depth and velocities on the flood flow in flood plain where submerged/non-submerged topography are presented. The verification demonstrates that the model can reproduce the complex behavior of the flows with reasonable accuracy.

INTRODUCTION

In recent years, flooding due to high intensity rainfall has been increasing. In Japan, countermeasures against flooding have tended to shift flood hazard mitigation measures such as hazard maps, effective systems of emergency evacuation and control of flood flow with flood retarding plantations etc. Numerical models are instrumental in investigating and predicting possible flooding scenarios, which can then be used to formulate suitable flood hazard mitigation measures.

The behavior of flood flows is affected by complicated flood plain geometries with topography with depressions in the ground or hills, structures, as well as road networks. Therefore, a numerical model for simulating flood flows is required to evaluate correctly the effects of the floodplain geometries on the flow. There are existing flood simulation models, which take into consideration the effects of houses (Fukuoka et al. (6), Suetugi & Kuriki (16) and authors (14), (1), (15)), river and sewerage network (Kawaike et al.(8)), flood retarding plantations (authors (13)), submerged topography (Glaister(7), Bermudez & Vazquez(2)) and the topography, which is submerged/non-submerged according to flow phenomena (Bradford and Sanders(3), Liu et al.(9)) on the flows.

In modeling of submerged/non-submerged topography, the discretization method of bed slope term and the treatment of submerged/non-submerged (dry/wet) topography require particular attention. For discretization of bed slope term, the method based on characteristics of the two-dimensional shallow water equations, which are hyperbolic partial differential equations and generally used as governing equations of flood flows, is required. Glaister(7) and Bermudez & Vazquez(2) proposed the discretization method of bed slope term, but no quantitative verification based on experimental data was carried out. On the other hand, the treatment of submerged/non-submerged (dry/wet) topography was

proposed by Bradford & Sanders (3), Liu et al. (9), Zhao et al. (18) and Fraccarollo and Toro (5). All these models were constructed based on a structured grid system. In this system, in order to lay out of grids around complicated boundaries of geometry, a highly fine grid may be needed. This poses serious difficulties in laying out grids along a complicated boundary, and may also result in a increased computational time for sufficient accuracy.

These aforementioned problems can be overcome by using an unstructured grid system, wherein grid sizes may be varied in a computational domain to fit the local geometry. This enables to lay out grids around complicated geometries more easily and correctly than a structured grid system. The efficiency of an unstructured grid system for flooding simulation has gained recognition, and several models ((14), (1), (15), (8)) have been constructed based on the grid system.

In this study, a numerical model for 2D flood flows on a flood plain of topography, which may be submerged/non-submerged depending on flow conditions, is developed. The model is based on the Spatial Averaged Finite volume method on Unstructured grid using FDS(Flux-Difference Splitting) technique for 2D Flood flows (SA-FUF-2DF model(13)). To treat flood flows on complicated topography, an upwind treatment of bed slope terms and a procedure for the movement of a wet/dry boundary are incorporated into the model. The model is applied to the experiment of the solitary wave which passes around a conical island, and then is verified against the experimental data of depths and velocities of the flood flow in flood plain with not only submerged topography but also with non-submerged topography.

NUMERICAL MODEL

SA-FUF-2DF Model

The SA-FUF-2DF model is the same as reference (13), and hence an outline of the model is briefly presented here.

The SA-FUF-2DF model (13) uses the following spatial averaged 2D shallow water equation as the governing equation

$$\frac{\partial \boldsymbol{U}}{\partial t} + \frac{\partial \boldsymbol{E}}{\partial x} + \frac{\partial \boldsymbol{F}}{\partial y} + \boldsymbol{S} = \boldsymbol{0} \tag{1}$$

where $\boldsymbol{U}$ = flow vector; $\boldsymbol{E}$ and $\boldsymbol{F}$ = flux vectors; $\boldsymbol{S}$ = vector containing source and sink terms. These vectors are given by

$$\boldsymbol{U} = \begin{pmatrix} h \\ uh \\ vh \end{pmatrix}; \boldsymbol{E} = \begin{pmatrix} uh \\ u^2h + \frac{1}{2}gh^2 \\ uvh \end{pmatrix};$$
$$\boldsymbol{F} = \begin{pmatrix} vh \\ uvh \\ v^2h + \frac{1}{2}gh^2 \end{pmatrix}; \boldsymbol{S} = \begin{pmatrix} 0 \\ -gh\left(S_{ox} - S_{fx}\right) + F_x \\ -gh\left(S_{oy} - S_{fy}\right) + F_y \end{pmatrix} \tag{2}$$

where t=time; h = flow depth; u, v = flow velocities along x- and y-direction, respectively; g = acceleration due to gravity; S_{ox} and S_{oy} = bed slopes along x- and y-direction (= $-\partial z_b/\partial x$ and $-\partial z_b/\partial y$), respectively; z_b = bed elevation; S_{fx} and S_{fy} = friction slopes along x- and y-direction (= $n^2 u\sqrt{u^2+v^2}/h^{4/3}$ and $n^2 v\sqrt{u^2+v^2}/h^{4/3}$), respectively; n = Manning's roughness coefficient; F_x and F_y = the drag forces due to obstructions within control volume.

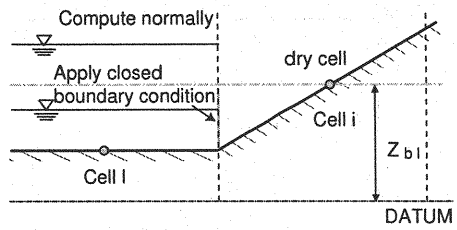

Fig.1 Sketch of partially dry cell

The integral form of the governing equations is obtained by integrating Eq.1 over a control volume Ω using the Gauss divergence theorem as

$$\frac{\partial}{\partial t}\int_{\Omega} \boldsymbol{U} dS + \oint_{\partial\Omega} (\boldsymbol{\mathcal{F}} \cdot \boldsymbol{n}) dL + \int_{\Omega} \boldsymbol{S} dS = \boldsymbol{0} \tag{3}$$

where $\boldsymbol{n}$ = outward-pointing unit vector normal to the cell face $\partial\Omega = (n_x, n_y)$; $\boldsymbol{\mathcal{F}} \cdot \boldsymbol{n} = \boldsymbol{E}n_x + \boldsymbol{F}n_y$ is normal flux vector; dL = length of $\partial\Omega$, dS = area of Ω.

Eq.3 is numerically integrated by using the unstructured finite volume discretisation and a forward Euler time discretisation. Also, the numerical flux through the cell faces is calculated by flux-difference splitting (FDS) technique (11). An unstructured triangle grid to correctly model complicated and well-developed urban areas with buildings, houses and other structures, which are treated as closed boundaries, is used. The time step is computed based on CFL type stability conditions expressed as $\Delta t = C_r(\min(dr))/(2\max(c + \sqrt{u^2+v^2}))$, where C_r = Courant number, c=celerity($=\sqrt{gh}$) and dr = length of vector joining the two centroids of a triangular grid cell.

Treatment of Bed Slope Terms

Following the argument of Roe (12) for linear equations, the terms containing space derivative in $\boldsymbol{S}$ should be upwinded in the same way as the flux term. Thus $\boldsymbol{S}_i$ is first split into portions with and without the space derivative terms. Thus,

$$\boldsymbol{S}_i = \boldsymbol{S}_{si} + \frac{1}{V_i}\sum_{k=1}^{N_e} \boldsymbol{S}_k^* \tag{4}$$

where $\boldsymbol{S}_{si}$ = the vector which contains no derivative term and $\boldsymbol{S}_k^*$ = upwinded vector which contains derivative term, V_i= area of cell i, N_e = total number of cell face (N_e=3 in case of triangular cells), i= index for cell, k= index for cell face. $\boldsymbol{S}_{si}$ and $\boldsymbol{S}_k^*$ can be written as

$$\boldsymbol{S}_{si} = \begin{pmatrix} 0 \\ ghS_{fx} + F_x \\ ghS_{fy} + F_y \end{pmatrix}_i \; ; \; \boldsymbol{S}_k^* = \frac{1}{2}\left(\tilde{\boldsymbol{S}}_k - \sum_{j=1}^{3}\left(\frac{|\tilde{\lambda}^j|}{\tilde{\lambda}^j}\,\tilde{\beta}^j\,\tilde{\boldsymbol{e}}^j\right)_k\right) \tag{5}$$

$\tilde{\boldsymbol{S}}_k$, $\tilde{\beta}^j$, $\tilde{\lambda}^j$, $\tilde{\boldsymbol{e}}^j$ in Eq.5 can be expressed as

$$\tilde{\boldsymbol{S}}_k = \begin{pmatrix} 0 \\ g\tilde{h}\,(L_k \Delta z_b n_x) \\ g\tilde{h}\,(L_k \Delta z_b n_y) \end{pmatrix} \; ; \; \begin{pmatrix} \tilde{\beta}^1 \\ \tilde{\beta}^2 \\ \tilde{\beta}^3 \end{pmatrix} = \frac{g\tilde{h}\,(L_k \Delta z_b)}{2\tilde{c}} \begin{pmatrix} 1 \\ 0 \\ -1 \end{pmatrix} \tag{6}$$

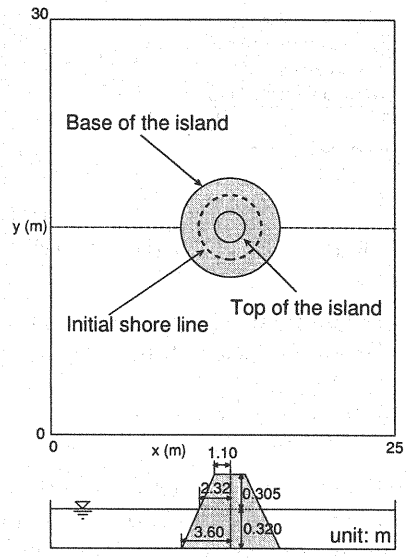

Fig.2 Experimental set-up for a solitary wave passes around a conical island (4)

$$\begin{pmatrix} \tilde{\lambda}^1 \\ \tilde{\lambda}^2 \\ \tilde{\lambda}^3 \end{pmatrix} = \begin{pmatrix} \tilde{u}n_x + \tilde{v}n_y + \tilde{c} \\ \tilde{u}n_x + \tilde{v}n_y \\ \tilde{u}n_x + \tilde{v}n_y - \tilde{c} \end{pmatrix}$$

$$\tilde{e}^1 = \begin{pmatrix} 1 \\ \tilde{u} + \tilde{c}n_x \\ \tilde{v} + \tilde{c}n_y \end{pmatrix} \; ; \; \tilde{e}^2 = \begin{pmatrix} 0 \\ -\tilde{c}n_y \\ \tilde{c}n_x \end{pmatrix} \; ; \; \tilde{e}^3 = \begin{pmatrix} 1 \\ \tilde{u} - \tilde{c}n_x \\ \tilde{v} - \tilde{c}n_y \end{pmatrix}$$

where L_k = length of k$^{\text{th}}$ face, c=wave speed $(=\sqrt{gh})$, Δ = operator defined as $\Delta(\bullet) = (\bullet)_R - (\bullet)_L$, $\tilde{u} = (\sqrt{h_L}u_L + \sqrt{h_R}u_R)/(\sqrt{h_L} + \sqrt{h_R})$, $\tilde{v} = (\sqrt{h_L}v_L + \sqrt{h_R}v_R)/(\sqrt{h_L} + \sqrt{h_R})$, $\tilde{h} = (h_L + h_R)/2$.

Treatment of wet/dry boundaries

FDS cannot estimate the numerical flux when the flow depth is zero. In this case, the computation cannot be continued. To circumvent this, a very small flow depth h_v is assumed in case of zero flow depth. The cell, in which the flow depth is less than h_v, is referred to a dry cell.

There are two types of dry cells: a fully dry cell and a partially dry cell. The fully dry cell is defined as the one with no adjoining cell where the flow depth is more than h_v. In case of fully dry cell, the flow depth h is set to h_v and the flow velocities u, v are set to zero. On the other hand, the partially dry cell is defined as the one with least one but not more than three adjoining cell, where the flow depth is more than h_v. In case of the partially dry cell, the flow depth and velocities are computed based on the relationships between bed elevation of a partially dry cell and water level of an adjoining cell. When the water level of an adjoining cell is greater than bed elevation of partially dry cell, the numerical flux is calculated by the FDS technique. When the water level of an adjoining cell is less than bed elevation of a partially dry cell, the closed boundary is applied to the interface of the cells.

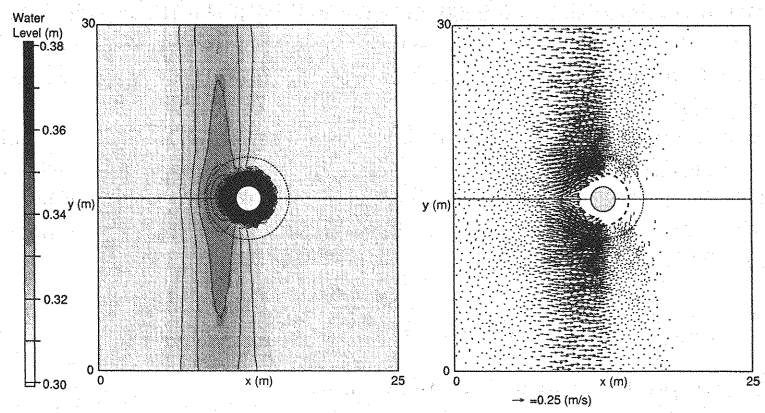

(a) $t = 8$ (s)

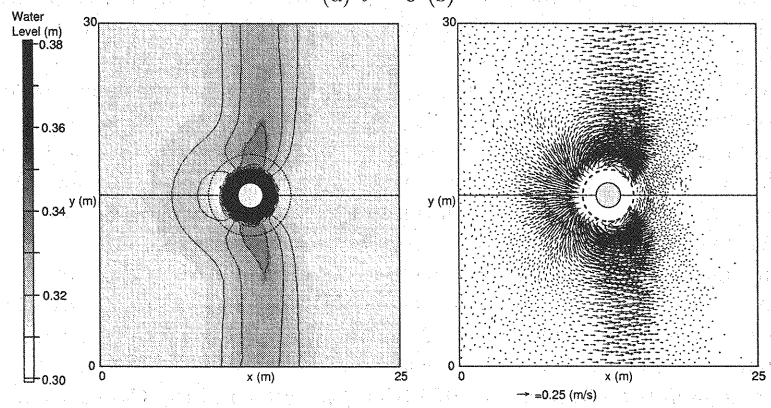

(a) $t = 10$ (s)

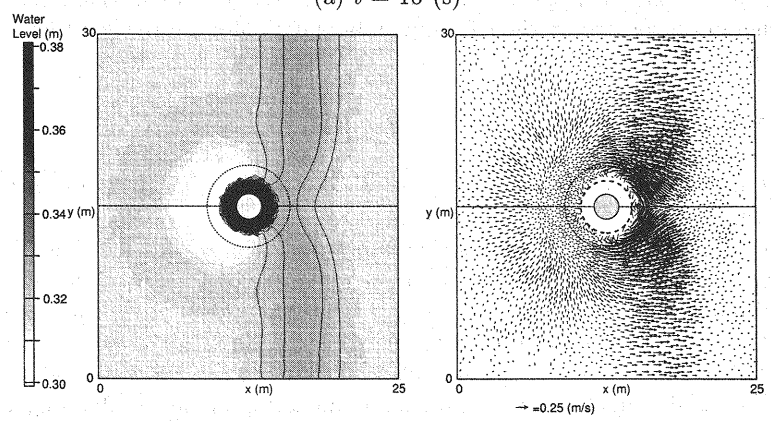

(a) $t = 12$ (s)

Fig.3 Numerical results of contours of water level and flow vectors (a solitary wave passes around a conical island)

Numerical experiments on 1D dam-break flows shows that the SA-FUF-2DF model always yields stable results if the floodplain tail water depth remains above h_v=0.00001m. The computed results with h_v=0.00001m agree well with the Ritter solutions (10) except near the wave front, and mass is conserved within a cumulative error of the order of 10^{-6}%. Based on these 1D results, the value of h_v=0.00001m is assumed to be valid for 2D computations.

In case of a very small flow depth, the bed friction computed by the Manning formula may become unrealistically high. In such cases, the bed friction is set to zero wherever the flow depth remains below 0.001m. It was confirmed by means of numerical experiments that the simulations continued stably with this treatment when the Manning's roughness n was under 0.07.

MODEL VERIFICATION

Solitary wave passes around a conical island

The SA-FUF-2DF model was first applied to the existing experimental data on a solitary wave which passes around a conical island. This was carried out by Briggs et al. (4). The data have been used by other investigators ((9), (17),(3)) as a test problem. As pointed out by Bradford and Sanders (3), depending on the model structure and treatment of dry/wet boundary, the spurious oscillations in computed water level and velocity vectors occur during the run-down of the wave around the dry/wet boundary and the computation cannot be continued owing to the oscillations. From such a point of view, the robustness of the SA-FUF-2DF model for simulating long wave run-up and run-down on arbitrary two-dimensional topography will be examined in the next section.

The calculation domain is 30m wide and 25m long. The center of a conical island was located at a center of the domain. The island is 0.625m high and has a base diameter equal to 7.2m and a top diameter of 2.2m. The still water depth h over the flat portion of the domain is 0.32 m. A sketch of the island geometry is shown in Fig.2.

The domain is discretized by 5076 triangular cells and the Courant number is set to 0.9. The bed friction is neglected as Liu et al. (9) carried out in their simulations. The wave generator is located on the left domain boundary and a water level η is given in Eq.7 as a boundary condition.

$$\eta = H\mathrm{sech}^2\left(\frac{C_s(t-T)}{l_s}\right) \tag{7}$$

where H = wave height(=0.032 m); $C_s = \sqrt{gh}\,(1 + H/(2h))$; $l_s = h\sqrt{4hc_s/(3H\sqrt{gh})}$; T = time at which the wave crest enters the domain (=2.45 s).

Fig.3 shows the computed water level and flow vectors at each time. It can be seen that the wave reaches the front of the island (Fig.3 (a)), and then the wave obstructed by the island is deflected(Fig.3 (b)), and consequently passes around the island(Fig.3 (c)). Spurious oscillations at computed water levels and unphysical velocity vectors during the rundown of the wave do not occur in the SA-FUF-2DF model. This provides evidence that the SA-FUF-2DF model is robust enough for simulating process of flooding and recession.

Flood wave passes over submerged and around non-submerged topograpy

The SA-FUF-2DF model is now applied to our experimental data on a flood wave, which passes over submerged and around non-submerged topography.

The experimental set-up consists of a reservoir and a flood plain as shown in Fig.4. The beds of both the reservoir and the flood plain, which are made of acrylic boards, are

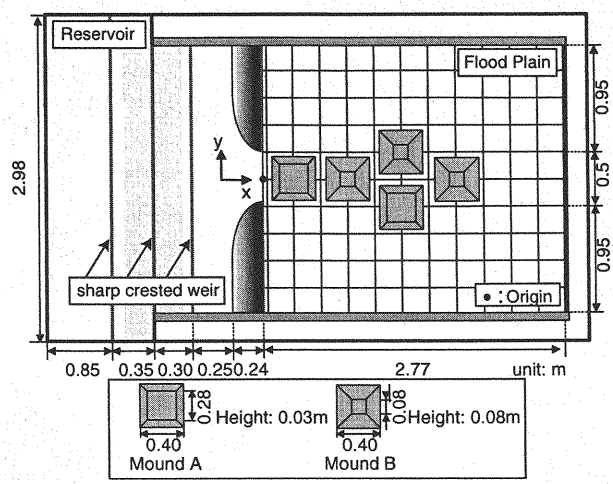

Fig.4 Experimental set-up and arrangement of mounds which is modeled on the topography

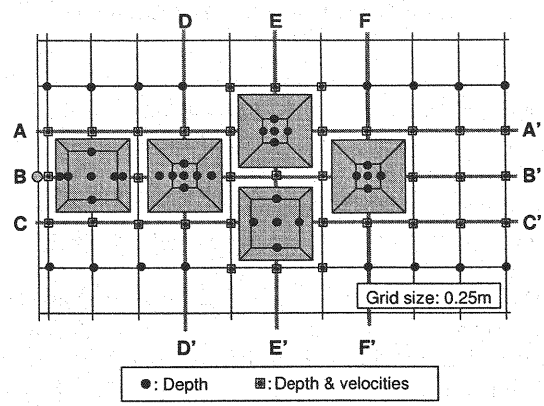

Fig.5 Observation stations

Table1 Experimental conditions for flood waves

Case	Discharge Q (m^3/s)	Height of downstream sharp crested weir (m)
I	0.0155	0.08
II	0.0155	0.04

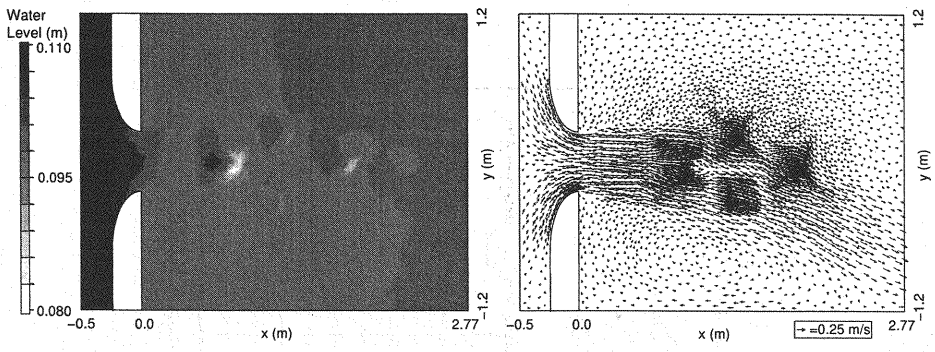

Fig.6 Numerical results of water level contours and velocity vectors (Case I : submerged)

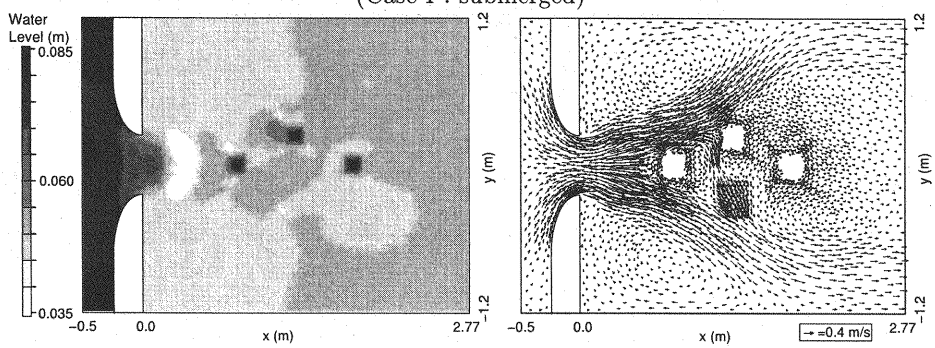

Fig.7 Numerical results of water level counters and velocity vectors (Case II : submerged/non-submerged)

set horizontally. A sharp crested weir (2.38m long) was placed at the downstream of flood plain. As shown in Fig.4, the two types of mound were used as topography.

Two cases of experiments were conducted; Case I was for verification against flood flows over the submerged topography; Case II was for verification against flood flows over submerged as well as non-submerged topography. The experimental conditions are given in Table1.

The flow depths and velocities were observed at each observation station specified in Fig.5. Flow depths h were observed by means of a wave height meter. The depth averaged flow velocities in x-direction u and in y-direction v were calculated by dividing a unit width discharge in x-direction q_x and y-direction q_y by depth h. The discharge q_x and q_y was obtained by integrating velocity profiles in x- and y-direction, which were obtained from flow velocity in x-direction u_x and in y-direction u_y observed by electromagnetic velocimeter

The domain is discretized by 3986 triangular cells and the Courant number is set to 0.9. Manning's roughness coefficient was set to 0.01 for acrylic bed. The unit width discharge (q=6.5$\times$ 10^{-3} (m^2/s)) is given as an upstream boundary condition, while the flow depth h=0.1m for Case I or h=0.056m for Case II is given as a downstream boundary condition. The closed boundary condition is applied on the side boundaries of the domain. As initial conditions, the velocities u and v are set to zero, while water levels are set to two states; one water level is set at a higher level than the both Mound A and B, the other water level is set at a lower level than the Mound B, although the steady state computational results obtained from two different initial conditions were found to be identical.

As pointed out by Bradford and Sanders (3), significant mass error is occurred

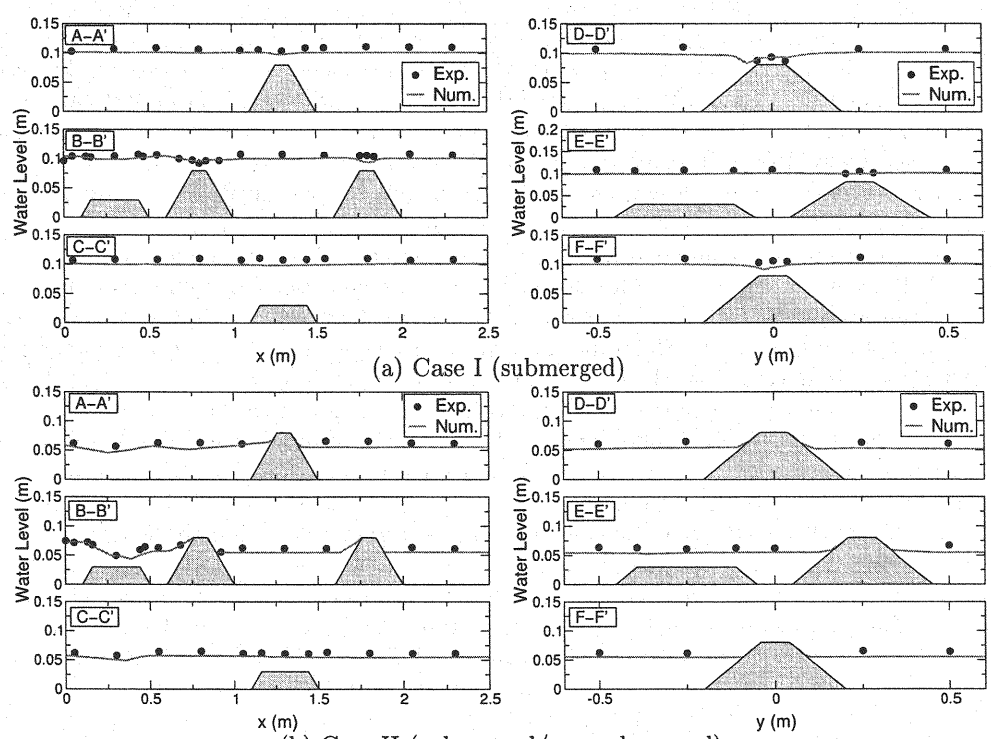

(a) Case I (submerged)

(b) Case II (submerged/non-submerged)

Fig.8 Comparison of computed and observed water level on each section in Fig.5

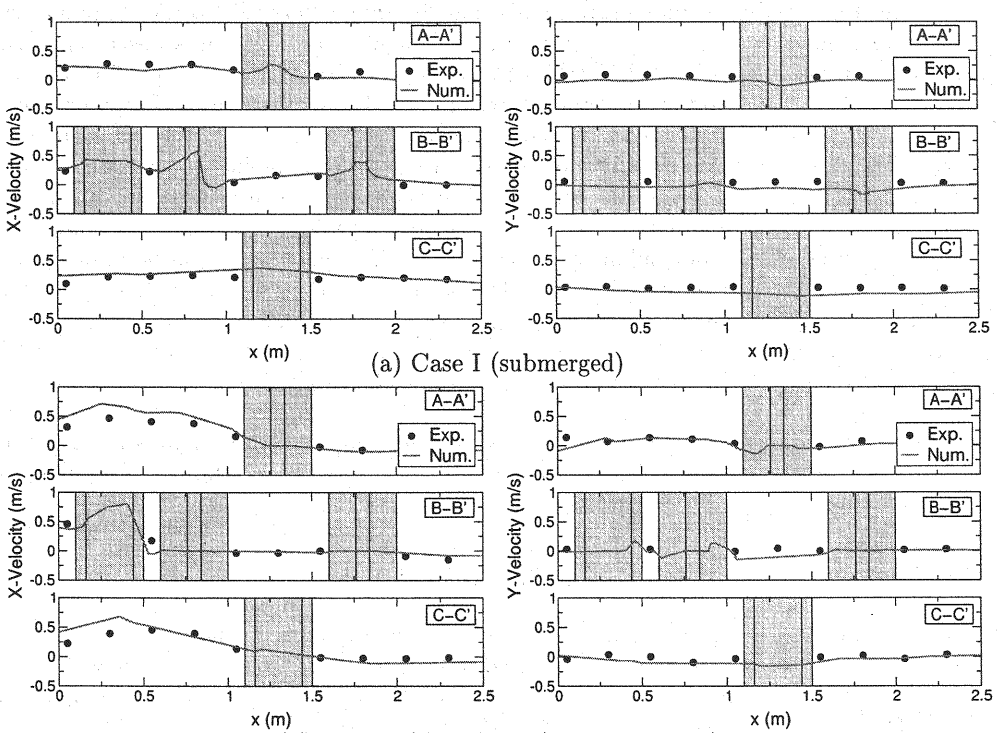

(a) Case I (submerged)

(b) Case II (submerged/non-submerged)

Fig.9 Comparison of computed and observed x, y-velocities on each section shown in Fig.5

when a treatment of wet/dry boundaries is inadequate, and then the flood propagation is underestimated because of the mass error. In the treatment used in this study, the mass error remains from 1.0×10^{-6} to 3 %, and the error is acceptable for engineering standards.

Fig.6 and Fig.7 show computed water level and flow velocity vectors for Case I and II, respectively. It was observed that in Case I the velocity vectors are deflected due to the differences of topography height and in Case II the flood flow is divided by the topography located at the intersection of cross section B-B' and D-D' shown in Fig.5.

Fig.8 compares computed water levels with observed ones in the cross sections A-A' ~ F-F' shown in Fig.5. In both Case I and Case II, the computed results reproduce the experimental data adequately. In particular, the water surface profile is depressed over the topography in Case I, and the water level rose in front of the non-submerged topography whereas it dropped behind the non-submerged topography in Case II.

Fig.9 compares computed velocities with observed ones in the cross sections A-A' ~ C-C'. The shadow in Fig.9 illustrates the locations of the topography. In Case I, u over the topography located at the intersection of section B-B' and D-D' increase and then decrease through the topography. In Case II, u in the cross section B-B' increases over the submerged topography in the upstream and decreases rapidly, due to the effect of non-submerged topography located at the intersection of the cross section B-B' and D-D' on the flow. In both cases, the computed results reproduce the experimental data adequately.

The results mentioned above demonstrate that the SA-FUF-2DF model with treatment of wet/dry boundaries can predict well the depths and velocities of 2D flood flows under the presence of non-submerged as well as over submerged topography.

CONCLUSION

In this study, a numerical model for 2D flood flows in a flood plain with submerged/non-submerged topography was developed. The model was based on Spatial Averaged Finite volume method on Unstructured grid using FDS technique for 2D Flood flows (SA-FUF-2DF model). An upwind treatment of bed slope terms and a procedure for the movement of a wet/dry boundary were incorporated into the SA-FUF-2DF model to treat flood flows on complicated topography. The model was applied to the experiment of the solitary wave which passes around a conical island, and then was verified against the experimental data of depth and velocities of the flood flow in a flood plain with submerged topography as well as non-submerged topography. The model verification demonstrates that the model can reproduce the complex behavior of the flows in a flood plain with submerged as well as non-submerged topography with reasonable accuracy.

ACKNOWLEDGMENTS

This study was supported by Research Fellowships of the Japan Society for the Promotion of Science for Young Scientists. The authors wish to thank the contribution made by Mr. Toshihiko Kobayashi and Mr. Kazumasa Oota.

REFERENCES

1. Akiyama, J., Shige-eda, M. and Ura, M.: First- and second-order accurate 2D numerical model based on unstructured finite-volume method for flood flows, *Journal of Hydraulic, Coastal and Environmental Engineering,* JSCE, No. 705/II-59, pp. 31–43, 2002, (in Japanese).

2. Bermudez, A. and Vazquez, M.: Upwind methods for hyperbolic conservation laws with source terms, *Computers & Fluids*, Vol. 8, No. 8, pp. 1049–1071, 1994.

3. Bradford, S. F. and Sanders, B. F.: Finite-volume model for shallow-water flooding of arbitrary topography, *Journal of Hydraulic Engineering,* ASCE, Vol. 128, No. 3, pp. 289–298, 2002.

4. Briggs, M. J., E., S. C., Harkins, G. S. and Green, D. R.: Laboratory experiments of Tsunami runup on a circular island, *Pure Applied GeoPhysics*, Vol. 144, pp. 569–593, 1995.

5. Fraccarollo, L. and Toro, E. F.: Experimental and numerical assessment of the shallow water model for two-dimensional dam-break type problems, *Journal of Hydraulic Research*, Vol. 33, No. 6, pp. 843–864, 1995.

6. Fukuoka, S., Kawashima, M., Yokoyama, H. and MIzuguchi, M.: The numerical simulation model of flood induced flows in uraban residential area and the study of damage reduction, *Journal of Hydraulic, Coastal and Environmental Engineering,* JSCE, No. 600/II-44, pp. 23–36, 1998, (in Japanese).

7. Glaister, P.: Approximate Riemann solutions of shallow water equations, *Journal of Hydraulic Research*, Vol. 26, pp. 293–306, 1988.

8. Kawaike, K., Inoue, K., Toda, K. and Nakagawa, Y.: Inundation flow analysis in urban area applied to Neya river basin, *Advances in River Engineering*, Vol. 8, pp. 37–42, 2002, (in Japanese).

9. Liu, L. P., Cho, Y., Driggs, M., Kanoglu, U. and Synolakis, C.: Runup of solitary waves on a circular island, *Journal of Fluid Mechanics*, Vol. 302, pp. 259–285, 1995.

10. Ritter, A.: Die fortpflanzung der wasserwellen, *Zeitschrift des Vereines Deutscher Ingenieure*, Vol. 36 (33), pp. 947–954, 1892.

11. Roe, P. L.: Approximate Riemann solvers, parameter vectors and difference schemes, *Journal of Computational Physics*, Vol. 43, pp. 357–372, 1981.

12. Roe, P. L.: Upwind differencing schemes for hyperbolic conservation laws with source terms, *1st International Conference on Hyperbolic Problems, ST. Etienne*, pp. 41–51, 1986.

13. Shige-eda, M. and Akiyama, J.: Numerical investigation of flood control functions of flood retarding plantations, *Journal of Hydraulic, Coastal and Environmental Engineering,* JSCE, No. 740/II-64, pp. 19–30, 2003, (in Japanese).

14. Shige-eda, M., Akiyama, J., Ura, M. and Arita, Y.: 2D Numerical model based on unstructured finite volume method for flood flows, *Annual Journal of Hydraulic Engineering,* JSCE, Vol. 45, pp. 895–900, 2001, (in Japanese).

15. Shige-eda, M., Akiyama, J., Ura, M. and Kobayashi, T.: Numerical simulation of flood flows and hydrodynamic forces acting on structures, *Annual Journal of Hydraulic Engineering,* JSCE, Vol. 46, pp. 833–838, 2002, (in Japanese).

16. Suetugi, T. and Kuriki, M.: Research on Application for flood disaster prevention and simulation of flooding flow by means of new flood simulation model, *Journal of Hydraulic, Coastal and Environmental Engineering,* JSCE, No. 593/II-44, pp. 41–50, 1998, (in Japanese).

17. Titov, V. V. and Synolakis, C. E.: Numerical modeling of tidal wave runup, *ournal of Waterway, Port, Coastal, and Ocean Engineering,* ASCE, Vol. 124 (4), pp. 157–171, 1998.

18. Zhao, D. H., Shen, H. W., Tabios III, G. Q., Lai, J. S. and Tan, W. Y.: Finite volume two-dimensional unsteady-flow model for river basins, *Journal of Hydraulic Engineering,* ASCE, Vol. 120, No. 7, pp. 863–883, 1994.

APPENDIX-NOTATION

The following symbols are used in this paper:

c	=	celerity($=\sqrt{gh}$);
dL	=	length of $\partial\Omega$;
dS	=	area of Ω;
$\boldsymbol{E}$, $\boldsymbol{F}$	=	flux vectors;
F_x, F_y	=	the drag forces due to obstructions within control vloume;
$\boldsymbol{\mathcal{F}} \cdot \boldsymbol{n}$	=	normal flux vector;
g	=	acceleration due to gravity;
h	=	flow depth;
i	=	index for cell;
k	=	index for cell face;
L_k	=	length of k^{th} face;
n	=	Manning's roughness coefficient;
$\boldsymbol{n}$	=	outward-pointing unit vector normal to cell face = $((n_x, n_y))$;
N_e	=	total number of cell face;
$\boldsymbol{S}$	=	vector containing source and sink terms;
S_{fx}, S_{fy}	=	friction slopes along x- and y-direction, respectively;
$\boldsymbol{S}_k^*$	=	upwinded vector which contains derivative term;
$\boldsymbol{S}_{si}$	=	the vector which contains no derivative term;
S_{ox}, S_{oy}	=	bed slopes along x- and y-direction, respectively;
t	=	time;
$\boldsymbol{U}$	=	flow vector;
u, v	=	velocities along x- and y-direction, respectively;
V_i	=	area of cell i;
z_b	=	bed elevation; and
Ω	=	control volume.

(Received September 19, 2003 ; revised November 25, 2003)